



FULL LENGTH ARTICLE

DNA damage-mediated cellular senescence promotes hand-foot syndrome that can be relieved by thymidine prodrug



Bingxue Yang ^{a,1}, Xinran Xie ^{b,1}, Zhaoyu Wu ^b, Dazhao Lv ^b,
Jiajun Hu ^b, Yuyun Chen ^b, Jiaxing Li ^b, Shuyue Luo ^b,
Jiacheng Li ^b, Jie Luo ^{b,*}, Shiyi Zhang ^{b,**}

^a School of Pharmacy, Shanghai Jiao Tong University, Shanghai 200240, China

^b School of Pharmacy and School of Biomedical Engineering, Shanghai Jiao Tong University, Shanghai 200240, China

Received 17 February 2022; received in revised form 7 October 2022; accepted 8 October 2022

Available online 18 October 2022

KEYWORDS

Cellular senescence;
cGAS-STING;
Cutaneous toxicity;
DNA damage;
Fluoropyrimidine;
Hand-foot syndrome;
Keratinocytes;
Thymidine prodrug

Abstract Hand-foot syndrome (HFS) is a widely recognized dose-limiting cutaneous toxicity effect of fluoropyrimidine chemotherapy agents that impairs clinical benefits and treatment outcomes. Even though the cause and pathophysiology of HFS are relatively widely reported, how the toxicity of fluoropyrimidine translates into persistent inflammation has not been studied. Additionally, prevention and treatment strategies for HFS based on its mechanistic occurrence and development are scarce. In our study, we demonstrated that cGAS-STING signaling pathway-mediated cellular senescence played a critical role in the inflammatory reaction and provided a therapeutic solution for HFS. Mechanistically, DNA damage, as the primary cytotoxic cause, in keratinocytes induces cell cycle arrest, activates the cGAS-STING signaling pathway, and subsequently mediates cellular senescence, ultimately fueling a robust secondary inflammatory response that results in HFS. More importantly, the thymidine prodrug thymidine diacetate was proven to be effective in preventing HFS by compensating for thymidylate deficiency to facilitate the replication and repair of DNA and thus causing the escape from cellular senescence. These data highlight the importance of DNA damage-mediated cellular

* Corresponding author.

** Corresponding author.

E-mail addresses: jieluo@sjtu.edu.cn (J. Luo), zhangshiyi@sjtu.edu.cn (S. Zhang).

Peer review under responsibility of Chongqing Medical University.

¹ These authors contributed equally to this work.

senescence in the etiology of HFS and provide a potential therapeutic anchor point for fluoropyrimidine-induced HFS.

© 2022 The Authors. Publishing services by Elsevier B.V. on behalf of KeAi Communications Co., Ltd. This is an open access article under the CC BY-NC-ND license (<http://creativecommons.org/licenses/by-nc-nd/4.0/>).

Introduction

Fluoropyrimidines, mainly 5-fluorouracil (5-FU), capecitabine, and S-1, are a classical type of chemotherapy agent and are widely used for the treatment of several malignancies.¹ Hand-foot syndrome (HFS), also known as palmar-plantar erythrodysesthesia, is dose-limiting toxicity.^{2,3} Clinical manifestations of HFS include a prodrome of dysesthesia on the palms and soles, followed by painful, symmetric, well-defined erythema and edema.^{4,5} If the chemotherapy agent is not discontinued or decreased to a lower dose after the onset of HFS, skin breakdown may occur, accompanied by desquamation, bullous formation, or secondary infection, resulting in severe HFS cases.^{6,7} The incidence of any grade of HFS with infusional 5-FU in phase 3 trials varies between 18% and 71.9%^{2,3}; with capecitabine, the incidence varies between 22% and 77%^{2,8}; and S-1 has a reported incidence ranging from 5.4% to 45%.^{9–11} Although not life-threatening, HFS can be unbearable and interfere with daily activities, thereby seriously compromising the quality of life.¹² Currently, the mainstay of HFS management is dose reduction or interruption,^{13–15} which may negatively impact the therapeutic efficacy of chemotherapy or even cause cancer progression.

Despite its common occurrence and essential role in anti-cancer treatment outcomes, the mechanism of HFS and how fluoropyrimidines translate into persistent inflammation are not well understood. Hence, there are currently limited intervention strategies for HFS. It is possible that cytostatic therapy can mediate the toxic effect on epidermal basal keratinocytes due to the high turnover rate of these cells.^{15,16} This hypothesis is supported by histological and structural investigations in which premature and irregular keratinization, basal vacuolization, and keratinocyte necrosis were found.^{15,17} The features of the affected epidermis are nonspecific disease phenotypes, which cannot elucidate any accurate pathogenetic mechanism. In addition, tissues affected by HFS show general inflammatory changes, such as dilated blood vessels, edema, and lymphocyte infiltration, but there is no evidence of a clear marker for the condition.¹⁵ As a result, fluoropyrimidine-associated HFS can only be treated empirically with symptomatic treatments.¹⁸ However, dose reduction or interruption is the only solution for patients bearing high-grade HFS.^{6,18} Therefore, the development of effective treatment approaches for HFS based on its mechanistic occurrence is urgently needed.

The mechanism of cytotoxicity of fluoropyrimidine is generally attributed to RNA damage occurring through the misincorporation of fluoronucleotides into RNA, and to DNA damage caused by the inhibition of the nucleotide synthetic enzyme thymidylate synthase.^{1,19,20} The significance of DNA and RNA damage in cytotoxicity and their contribution to the

development of HFS remain unclear. There have been reports of a difference in toxicity between bolus-injected and infusional 5-FU.^{21–24} Bolus-injected 5-FU is more likely to cause RNA damage,^{19,25} while DNA damage occurs more critically with the long-term infusion of 5-FU,^{24,26} which is similar to the effect of oral fluoropyrimidines.^{1,27,28} Compared with bolus injection, 5-FU administered by continuous infusion carries a much higher risk of HFS.²⁹ Therefore, we speculate that the dominant mechanism of 5-FU cytotoxicity in the development of HFS is more closely associated with DNA damage. DNA damage elicits various cellular responses and can lead to severe inflammation via different molecular mechanisms. Cellular senescence is one of the consequences of severe or irreparable DNA damage,³⁰ especially the activation of multiple signal pathways mediated by DNA strand breaks.³¹ Senescent cells are permanently withdrawn from the cell cycle and generally develop a persistent proinflammatory phenotype called the senescence-associated secretory phenotype (SASP).^{32,33} Because of SASP, persistent senescent cells are thought to accelerate the onset of diseases,³⁴ which could be associated with the development of HFS.

In this study, we sought to unravel the cellular mechanisms underlying fluoropyrimidine-induced HFS. To this end, using capecitabine as an example, we first developed a rat model of HFS. We demonstrated that DNA damage-mediated cellular senescence in keratinocytes promotes HFS. DNA damage induces cell cycle arrest, activates the cGAS-STING pathway, and results in cellular senescence, ultimately leading to a severe inflammatory response in the epidermis and dermis. Based on these findings, we further demonstrated that thymidine diacetate (TDA), a thymidine prodrug, could repair DNA damage, successfully decreasing the severity of HFS without compromising treatment efficacy. Taken together, our results identify a new mechanism and provide a promising mechanism-based therapeutic solution for the treatment of fluoropyrimidine-induced HFS.

Materials and methods

Study design

The objective of this study was to create a rat model of fluoropyrimidine-induced hand-foot syndrome that recapitulates patient phenotype and to demonstrate the efficacy of therapy using thymidine prodrug, thymidine diacetate. We started by generating rats that, upon capecitabine administration, perform HFS like symptoms in the palms. In all the *in-vivo* experiments, animals were randomly assigned to experimental or treatment groups and caretakers, and investigators conducting the experiments were blinded to the treatment allocations. Animal procedures were approved by local and national ethics

committees. In general, continuous data were analyzed by the Student's *t*-test, Mann–Whitney test, or analysis of variance (ANOVA).

Chemicals

Capecitabine was purchased from Goyic (China). 5-Fluorouracil (5-FU) was purchased from Abcam (England). Thymidine (TdR) and uridine (UR) were purchased from Sigma (USA). SN-011 was purchased from MCE (USA). Thymidine diacetate (TDA) and compounds 2a-4b were purchased from WuXi AppTec (China). Deoxyuridine monophosphate (dUMP) and deoxythymidine triphosphate (dTTP) standards were purchased from Sigma (USA). Vehicle, TdR, and TDA gel were made of propylene glycol, transcutol, PEG400, water, Carbopol 980, and 5% active ingredient. For *in-vitro* experiments, 5-FU was dissolved in PBS (Sangon, China). TdR, UR, TDA, and compounds 2a-4b were dissolved in DMSO (Sigma). For *in-vivo* experiments, capecitabine was dissolved in Cremophor EL/ethanol (50:50; Macklin Cremophor EL; 99% ethanol) at 4 × of the highest dose as the stock solution.

Animals

All experiments were conducted in accordance with protocols approved by the Center for Drug Safety Evaluation and Research of East China Normal University (China). All mice were bred according to the protocol of the Institutional Animal Care and Use Committee. Female Sprague–Dawley rats (aged 6–8 weeks and weighing 180–220 g) were purchased from Shanghai Laboratory Animal Research Center (China). Female BALB/c nude mice (aged 6–8 weeks and weighing 18–21 g) were purchased from Shanghai Jihui Laboratory Animal Care (China). Rats and mice were used for experiments after one week of rest. Animals were housed in groups ($n = 5$) on a standard 12 h/12 h light–dark cycle and supplied with autoclaved tap water and sterile pellets *ad libitum*.

HFS modeling and treatment

HFS model was generated by daily oral administration of capecitabine at a dose of 4,000 mg per kg of body weight for about 50 consecutive days. In terms of HFS grade, its presence could be evaluated as grade 0 (normal), grade 1 (slight desquamation or dry lines), grade 2 (peeling, blisters, edema or swelling), and grade 3 (ulceration, severe blistering, and erythema). For the prophylactic treatment study, rats were randomized into four groups, (i) control group treated with 1 × solution of Cremophor EL/ethanol/PBS (12.5: 12.5: 75) without capecitabine, (ii) CAP-vehicle group treated with capecitabine and topical gel without active ingredients, (iii) CAP-5% TdR group treated with capecitabine and topical gel with 5% TdR, and (iv) CAP-5% TDA group treated with capecitabine and topical gel with 5% TDA.

Von Frey test

This test was performed as described previously.¹¹ Briefly, a logarithmic series of 10 calibrated Semmes-Weinstein monofilaments (von Frey filaments; Stoelting, Wood Dale,

USA) were applied for 8 s randomly to the left and right hind paws of all animals in order to characterize the threshold stimulus intensity necessary to produce a paw withdrawal response. Log stiffness of the filaments was determined by \log_{10} (milligrams \times 10) and ranged from manufacturer designated 2.83 (0.07 g) to 5.18 (15.136 g) filaments. Behavioral responses were used to calculate the absolute threshold (the 50% paw withdrawal threshold) by fitting a Gaussian integral psychometric function using a maximum-likelihood fitting method as described previously by Milligan et al.¹¹

The xenograft tumor model

For mice study, 6-week-old female BALB/C nude mice were injected subcutaneously in the right axilla with 1×10^6 HCT 116 cells in a volume of 100 μ L PBS. Tumor volumes were measured in two dimensions with calipers and calculated with formula $(L \times W^2)/2$, where L is the length and W is the width of the tumor, respectively. After tumor formation in two weeks following tumor cell inoculation, the mice were randomized into three groups, (i) control group treated with 1 × solution of Cremophor EL/ethanol/PBS (12.5: 12.5: 75) without capecitabine. (ii) CAP-vehicle group treated with capecitabine and topical gel without active ingredients, and (iii) CAP-5% TDA group treated with capecitabine and topical gel with 5% TDA. Capecitabine was administered orally once daily for 21 consecutive days at a dose of 180 mg per kg of body weight starting in 200 μ L above mentioned 1 × solution. TDA or vehicle gel was topically applied on the hind paws of mice for 4 h once a day for 21 consecutive days, concomitant with the continuous daily oral administration of capecitabine. The body weight and tumor volume were recorded every two days. Mice were sacrificed and dissected to measure the tumor weight.

Cell lines and culture conditions

The spontaneously immortalized cell line HaCaT was cultured in Dulbecco's modified Eagle's medium (DMEM) (Hyclone) supplemented with 10% fetal bovine serum (FBS), 2.0 mM L-glutamine, 100 units/mL penicillin and 100 mg/mL streptomycin. Primary epidermal keratinocytes NHEK from neonatal foreskin were purchased from Guangdong Biocell Biotechnology (China) and cultured in KM medium (ScienCell) containing keratinocyte growth supplements (ScienCell). The human colon cancer cell line HCT-116 was purchased from the Chinese Academy of Sciences Cell Bank. HCT-116 was cultured in DMEM (Invitrogen) supplemented with 10% FBS, 100 units/ml penicillin and 100 mg/mL streptomycin. Cells were maintained in 5.0% CO₂ at 37 °C. All cell lines were routinely tested for mycoplasma contamination.

Cell counting kit-8

Cell counting kit-8 (CCK8, YEASEN, China) assay was used to assess cell viability. The HaCaT cells were seeded at 5×10^3 cells/well in 96-well plates for 24 h. Next, the HaCaT cells were treated with 5-FU and other compounds for 48 h. The cells were incubated with CCK8 solution (10 μ L per well)

for 1 h. The optical density of each well was measured using a multifunction microplate reader (Infinite M200 Pro, Tecan) at 450 nm absorbable wavelength. Assays were performed in triplicate via three independent experiments.

Cell cycle analysis

Flow cytometry was used to examine the distribution of the cell cycle phases in HaCaT using a cell cycle detection kit (51-66211E, BD Biosciences, USA). Briefly, HaCaT cells were seeded at 2×10^6 cells/well in a 6-well plate for 24 h. The treated cell groups were fixed in cold 70% ethanol overnight. The cell samples were then stained with 50 μ L PI (50 μ g/mL) for 30 min in the dark at 25 °C. The distribution of cell cycles was detected by a FACSCalibur (BD Biosciences, USA).

Quantitative reverse Transcription–PCR

Total RNA was isolated from rat skin HaCaT cells with TRIzol™ reagent (Invitrogen). RNA concentrations were determined on a Nanodrop ND-1000 spectrophotometer. One μ g total RNAs were used for cDNA synthesis with the ReverTra Ace qPCR RT Master Mix (FSQ-301, TOYOBO), according to the manufacturer's instructions. qRT–PCR assay was performed with the ABI 7500 Real Time-PCR System using SYBR Green Master Mix (YEASEN). Relative expression was calculated with the $\Delta\Delta$ CT method with GAPDH as the housekeeping gene. Sequences of the PCR primers used in this work are listed in Table 1.

Western blot

Cellular proteins were extracted with RIPA lysis buffer containing protease inhibitors and phosphatase inhibitors. Protein concentrations were measured by using a BCA protein assay kit (Thermo Fisher Scientific, USA). Protein samples were separated using 12.5% SDS-PAGE and transferred onto a polyvinylidene fluoride membrane (Millipore). Subsequently, membranes were blocked with 5% bovine serum albumin in

PBS for 1 h and the appropriate antibodies at suitable concentrations were incubated overnight at 4 °C. The blots were then incubated with secondary antibodies at room temperature for 1 h. After extensive washing in TBST, protein bands were revealed with Super Singal West FemtoMaximum Sensitivity Substrate (Thermo Fisher Scientific, Rockford, USA) and visualized with Bio-Rad ChemiDocXRS system (Bio-Rad, USA). The primary antibodies were as follows: anti-GAPDH (Proteintech, 60004-1-Ig), anti-p-ATM (Cell Signaling Technology, #5883), anti-p16 (Cell Signaling Technology, #80772), anti-p21 (Cell Signaling Technology, #2947), anti-cyclin E (Cell Signaling Technology, #4129), anti-cGAS (Cell Signaling Technology, #79978), anti-p-p53 (Cell Signaling Technology, #82530), anti-p-IRF3 (Cell Signaling Technology, #29047), anti-IRF3 (Cell Signaling Technology, #4302), anti-p-TBK1 (Cell Signaling Technology, #5483), and anti-TBK1 (Cell Signaling Technology, #3504).

Immunofluorescence

Cells were fixed in 4% PFA (paraformaldehyde) for 30 min at room temperature. After washing four times with PBS (5 min each time), the cells were permeabilized with 0.2% Triton X-100 for 15 min at room temperature. After immersing in a blocking buffer containing 3% bovine serum albumin for 1 h, the cells were then incubated with primary antibodies in PBST containing 0.1% Tween 80 and 3% bovine serum albumin overnight at 4 °C. After washing four times with PBST, the cells were incubated with Alexa Fluor 488-conjugated goat anti-rabbit secondary antibody (Thermo Fisher Scientific, A11034) for 1 h at room temperature. Then the cells were washed four times with PBST and mounted with mounting medium (ProLong Gold antifade mountant with DAPI, Invitrogen, P36962). Images were taken with 20 \times oil immersion objective lens at room temperature and image acquisition was performed using an upright/inverted Fluorescent Microscope 139 (Revolve, Echo). Digitized images were analyzed and processed through ImageJ software. Anti- γ -H2AX (Cell Signaling Technology, #9718) antibody was used.

Table 1 The primer sequences for polymerase chain reaction.

Gene	Forward	Reverse
Human GAPDH	TGCCCTCAACGACCACTTTG	TTCCTCTTGCTCTTGCTGGG
Human p16	ATGGAGCCTTCGGCTGACTG	CCATCATCATGACCTGGATCGG
Human p21	CCTGTCACTGTCTTGACCTTG	TGGTAGAAATCTGTCATGCTGGTC
Human cyclin E1	CTCCAGGAAGAGGAAGGCAAC	GTCATCATCTCTTTTTGTCAGGTGTG
Human IL-1 β	CGCCAGTGAATGATGGCTTATTAC	GTCGGAGATTCGTAGCTGGATG
Human IL-6	AACAACCTGAACCTTCCAAAGATG	GCTTGTTCCTCACTACTCTCAAAT
Human cGAS	ATCTGTGGATATAACCCCTGGCTTTG	AAATGGCTTTAGTCGTAGTTGCTTC
Human IFN- β	ACGCCGCATTGACCATCTAT	GTCTCATTCCAGCCAGTGCT
Rat GAPDH	AGGTCGGTGTGAACGGATTTG	GGGGTCGTTGATGGCAACA
Rat cyclin E1	CTCCGACCTTTCAGTCCGC	CACAGTCTTGTCATCTTGCCA
Rat p16	CCGATACAGGTGATGATGATGGG	TGCAGTACTACCAGAGTGCTAGG
Rat p21	CAAAGTATGCCGTCTGTCTGTT	CTCAGTGGCGAAGTCAAAGTTC
Rat IL-6	GTCATTACAGCAATACTGAAACCC	CAAGTGCTTTCAAGATGAGTTGGAT
Rat IL-1 β	AATGGACAGAACATAAGCCAACAAG	ACACAGGACAGGTATAGATTCTTCC
Rat cGAS	ATTACGAAACTGGTGCTTTCTATCG	AATGAGTTCCCTAAACTTTGACAGC

Senescence-associated β -galactosidase staining

β -Galactosidase staining was done with a senescence-associated β -galactosidase staining kit (Beyotime, China). Cells were washed three times with PBS and fixed with 4% paraformaldehyde for 15 min at room temperature. Next, the cells were incubated overnight at 37 °C (no CO₂) in the dark with the working solution containing 0.05 mg/mL 5-bromo-4-chloro-3-indolyl-b-D-galactopyranoside (X-gal). Under a light microscopic examination, dark-green color in the observed cells indicated positive for the activity of the cellular senescence marker β -galactosidase (SA- β -gal).

CyQUANT cell proliferation assay

HaCaT cells were seeded in 96-well plates at a density of 5×10^3 cells/well and allowed to attach for 12 h. Then, HaCaT cells were treated with 5-FU for 48 h. Cell proliferation was assessed by fluorometric quantification of DNA using CyQUANT Proliferation Assay Kit (Life Technologies, USA) according to the manufacturer's instructions. HaCaT cells (5,000 cells per well) were cultured in black 96-well plates with clear bottoms and were treated as indicated for 48 h. The supernatants were then removed by blotting on paper towels, and the plates with clear bottoms were subsequently frozen at -80 °C. The plates were then thawed at room temperature, and 200 μ L of CyQUANT dye/cell lysis buffer mixture was added to each well. After 5 min of incubation, fluorescence was measured at 490-nm excitation and 520-nm emission wavelengths using FlexStation 3 multimode microplate reader (Molecular Devices).

Comet assay

The alkaline comet assay (pH > 13) was used to measure DNA damage. For the analysis of DNA damage 24 h after the exposure, the samples were placed on ice and the cells were detached from petri dishes with 3 mL of 0.25% Trypsin in 0.02% EDTA in PBS. The samples with detached cells were suspended in PBS and then 15 μ L (approximately 1.5×10^4 cells) of the cell suspension was pipetted in 75 μ L of 0.5% low-melting-point agarose. After careful mixing, the suspension was layered onto a microscope slide (pre-coated with a thin layer of 1% normal-melting-point agarose), immediately covered with a coverslip and kept on ice for 5 min to solidify the agarose. The coverslips were carefully removed and the slides were immersed in a lysis solution (2.5 M NaCl, 100 mM Na₂EDTA, 10 mM Tris, 1% sodium lauroyl sarcosinate, 1% Triton X-100; pH = 10) and incubated for 1 h at 4 °C in the dark. The slides were then placed in a horizontal electrophoresis unit (Gibco-BRL, Horizon 20 \times 25, USA) for 25 min, allowing the DNA to unwind in the electrophoresis buffer (1 mM EDTA and 300 mM NaOH; pH = 13; 4 °C). The electrophoresis was run for 30 min at 24 V (0.66 V/cm) and 380 mA. After electrophoresis, the slides were neutralized (3 \times 5 min) with Tris buffer (0.4 M; pH = 7.5) and fixed in 96% ethanol for 1 min. For the assay, slides were coded and stained with 20 μ g/mL ethidium bromide. The analysis of 20 nuclei per slide was performed with a fluorescence microscope (Axio Imager. A1, Germany), using the comet assay IV (Perceptive Instruments, UK) image analysis software. Olive

tail moment (OTM; the product of the tail length and the fraction of total DNA in the tail) was used as the parameter of DNA damage.

Enzyme-linked immunosorbent assay

The protein levels of IL-1 β and IL-6 were measured using enzyme-linked immunosorbent assay (ELISA) kits (Boster, USA) according to the manufacturer's instructions. The plates were read at 450 nm using a multifunction microplate reader (Infinite M200 Pro, Tecan).

Histology, immunohistochemistry (IHC) and immunofluorescence (IF)

The paws were harvested from rats under different treatments. The rat paw tissues were fixed in 4% paraformaldehyde and embedded in paraffin for hematoxylin and eosin (H&E) staining and immunostaining. For H&E staining, paraffin sections were cut at 4 μ m and stained using standard methods. For immunohistochemical staining, 4 μ m of paraffin sections were air-dried and then incubated with Ki67 (1:100; DAKO), γ H2AX (1:100), CD3 (1:100), CD68 (1:100), IL-1 β (1:100), IL-6 (1:100), cyclin E (1:100), p16 (1:100) and p21 (1:100) at 4 °C overnight. The stained slides were rinsed with PBST and incubated with HRP labeled goat anti-rabbit or mouse IgG (1:200; Zsbio, China) for 30 min at room temperature. After a rinse with PBST, the slides were incubated with DAB (Zsbio, China) for visualization. Subsequently, the slides were counterstained with Harris' hematoxylin for 10 s and washed with tap water. EdU incorporation is detected by Click-It EdU Alexa Fluor 594 Imaging Kit (Invitrogen). Sections were visualized under a digital pathology scanning 138 system (NANOZOOMER S360, Leica) or an upright-inverted Fluorescent Microscope 139 (Revolve, Echo).

Evaluation of dUMP and dTTP levels *in vitro*

Cells were seeded in a 10-cm² Petri dish at 1×10^6 cells and pre-cultured for 24 h, prior to treatment with test compounds. At each time (0 h, 0.5 h, 1 h, 3 h, 6 h, 12 h, 24 h and 48 h), cells were collected and resuspended in 100 μ L cell lysis (Beyotime). The samples were diluted 2-fold with 46.5 μ L of blank lysis. An aliquot of 50 μ L of the sample was added with 150 μ L ACN containing ACU (20 ng/mL), ¹³C5-thymidine (100 ng/mL), verapamil (5 ng/mL), glibenclamide (50 ng/mL), diclofenac (200 ng/mL), tolbutamide (200 ng/mL), and 3,4-dihydroxybenzoic acid (200 ng/mL) for protein precipitation; the mixture was vortexed for 10 min and then centrifuged at 3,700 rpm for 8 min. Then 40 μ L of supernatant was mixed with 120 μ L water and vortexed for 10 min. An aliquot of 1 μ L of the mixture was injected into the LC-MS/MS system (Triple Quad 5500, Waters, USA). The procedures of sample treatments and other details can be found in published reports.^{35,36}

Statistical analyses

All data were expressed as the mean value \pm standard deviation (SD). When comparing two groups, Student's *t*-test (unpaired, two-tailed) was performed. For

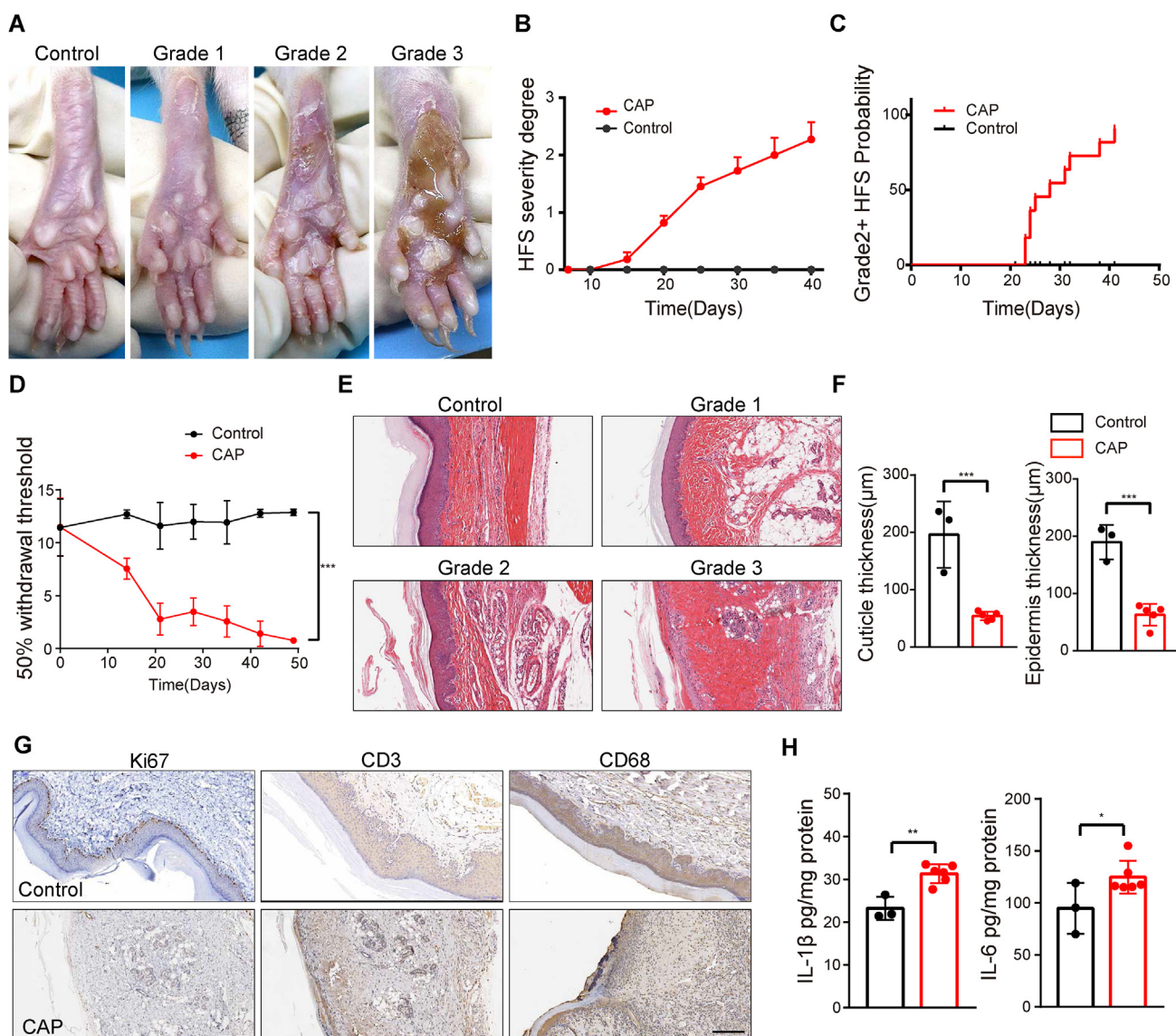


Figure 1 Rat model construction and pathology of HFS. (A) Representative images of paw grading in rats after oral gavage of capecitabine at a dose of 4,000 mg/kg of body weight. Mean HFS grade (B) and grade 2+ (C) HFS probability of rats ($n = 10$). (D) Mechanical pain thresholds were measured with von Frey filaments. Capecitabine-treated rats displayed bilateral mechanical pain hypersensitivity ($n = 5$). (E) H&E staining of graded paws of rats treated with capecitabine. (F) Quantitative analysis of epidermal damage was assessed by measuring the stratum corneum and epidermal thicknesses ($n = 5$). (G) Representative Ki67, CD3, and CD68 immunohistochemical staining images of rat paws. (H) IL-1 β and IL-6 concentrations in the rat paws were measured by ELISA ($n = 3$). Scale bar: 100 μ m. The results in (B), (C), (D), (F) and (H) are presented as the mean \pm SD. * $P < 0.05$, ** $P < 0.01$, *** $P < 0.001$. ns, no significant difference.

experiments in which one variable was analyzed for multiple conditions, one-way ANOVA was performed. Differences were considered significant when P -value was less than 0.05 (* $P < 0.05$, ** $P < 0.01$, *** $P < 0.001$).

Results

Keratinocyte damage and inflammation mediated fluoropyrimidine-induced HFS

Using capecitabine, we constructed a rat model of HFS to investigate the associated pathophysiological changes.

With a proper dose of orally administered capecitabine, rats developed obvious HFS symptoms over time. In line with the clinical manifestation of HFS patients,^{5,7,18} we classified the HFS symptoms of rats into three grades (Fig. 1A). As capecitabine treatment continued, severe HFS was found in almost all of the rats (Fig. 1B, C). Because painfulness is an essential standard used to classify grade 1 and grade 2 HFS in the clinic, we checked the mechanical allodynia of the rat paws (Fig. 1D). The pain tolerance thresholds of rat paws decreased as the oral gavage of capecitabine continued, which was consistent with the symptoms of HFS patients.^{7,12} H&E staining showed a thinned or even absent granular layer, a decrease in the

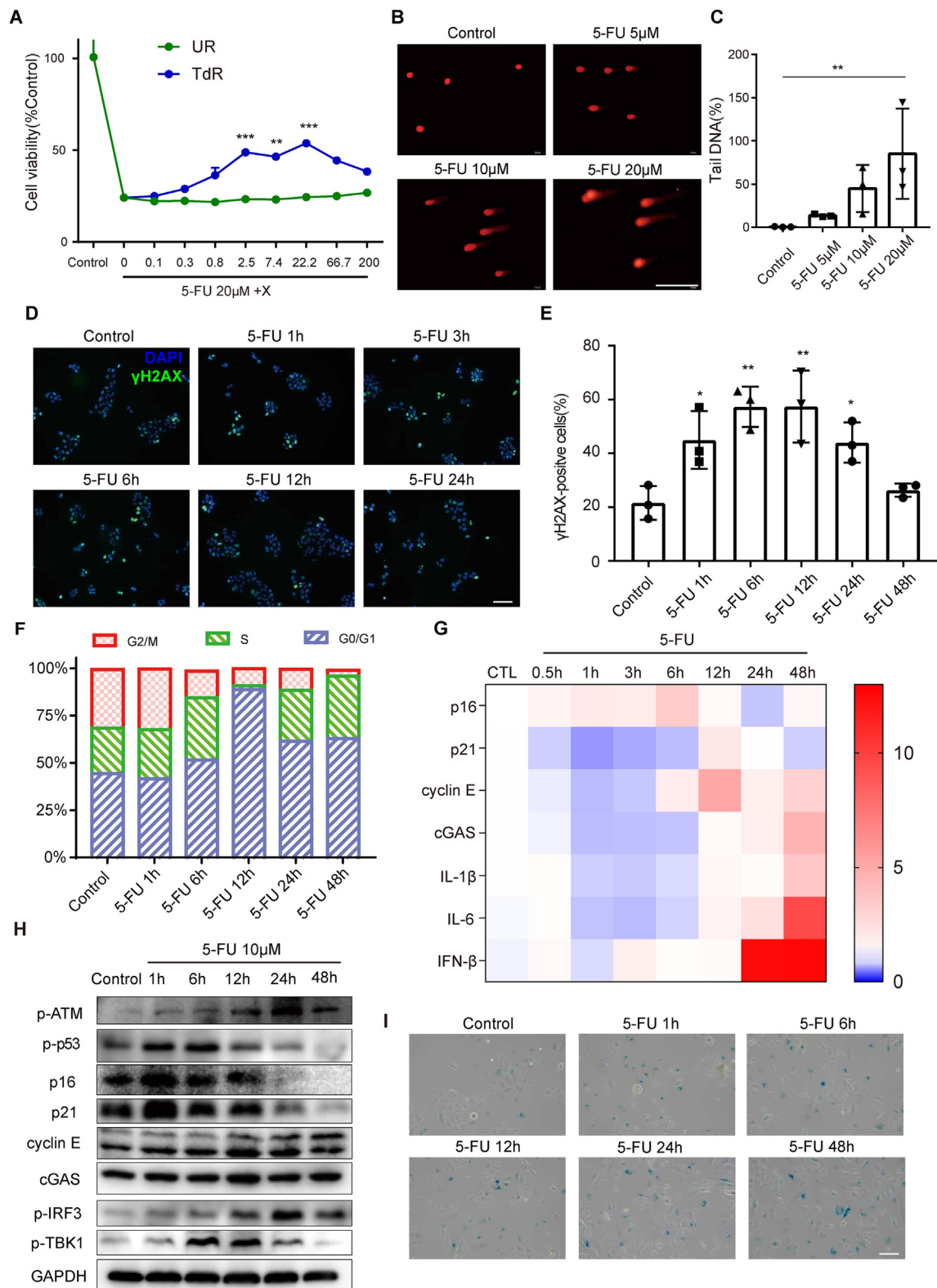


Figure 2 DNA damage-mediated cellular senescence is critical in fluoropyrimidine-induced HFS. **(A)** Effect of concurrent treatment with various concentrations of nucleosides (TdR, UR) on survival after exposure to 5-FU. Survival was measured by a Cyquant assay after 48-h exposure. The type of DNA damage in HaCaT cells was assessed by comet assays. Representative images **(B)** and **(C)** quantitative analysis results are shown ($n = 3$). **(D)** Degree of DNA damage revealed by γ H2AX immunofluorescence staining after 5-FU ($10 \mu\text{M}$) treatment for different periods. **(E)** Analysis of γ H2AX positive cells ($n = 3$). **(F)** Quantification of the cell cycle distribution in HaCaT cells after treatment with 5-FU ($10 \mu\text{M}$) represented by histograms. HaCaT cells were treated with 5-FU ($10 \mu\text{M}$), and subsequent changes in signaling pathways were assessed by quantitative RT-PCR **(G)**, ($n = 3$) and Western blot **(H)**

number of cells between the basal layer and the stratum spinosum, a rougher arrangement of cells, and thinning of the epithelial layer in HFS rats (Fig. 1E, F), indicating that the damage occurred mainly in the epidermis, especially in the keratinocytes in the basal layer. This finding agrees with the finding that keratinocytes are the primary cellular target of fluoropyrimidines.^{15,29} Meanwhile, dilated blood vessels, infiltrated lymphocytes and macrophages and the increased secretion of inflammatory factors (Fig. 1G, H; Fig. S1A–C) showed that capecitabine significantly triggered an inflammatory response.

DNA damage-mediated cellular senescence plays an important role in fluoropyrimidine-induced HFS

Since HFS is caused by cellular processes targeting keratinocytes, we used HaCaT and NHEK human keratinocyte cells to examine the mechanism of HFS *in vitro*. To determine the relative importance of DNA and RNA effects in the cytotoxicity of 5-FU to keratinocytes, we attempted to reverse cytotoxicity in HaCaT by supplying normal nucleosides (thymidine: TdR, uridine: UR) (Fig. 2A). The results showed that 5-FU cytotoxicity was efficiently reversed by TdR, while UR had very little effect. This suggests that 5-FU cytotoxicity was largely mediated by DNA damage in keratinocytes. Consistently, 5-FU was found to exert DNA damage early in treatment, as shown by γ H2AX immunofluorescence staining (Fig. 2D, E). We also conducted comet assays to investigate the extent of DNA damage (Fig. 2B, C). A higher concentration of 5-FU caused longer keratinocyte DNA tail, which indicated that 5-FU treatment exerts DNA damage in a dose-dependent manner. It was also found that the cell cycle was persistently arrested in HaCaT cells after exposure to 5-FU (Fig. 2F). Therefore, we examined DNA damage and cell cycle arrest markers in HaCaT and HFS rat models (Fig. 2G, H; Fig. S2A–E). The results indicated that 5-FU upregulated the transcription and expression of the corresponding genes. Reportedly, the cGAS/STING pathway is able to sense and respond to cytoplasmic DNA or micronuclei, both of which are indicative of damaged DNA that has escaped the nucleus.^{37–39} To investigate the role of this pathway in HFS, we examined the expression of cGAS and downstream pathway components during treatment. The results showed that 5-FU activated the cGAS-STING pathway in HaCaT cells and the rat model (Fig. 2G, H; Fig. S2B, G, I), suggesting that 5-FU-induced DNA damage could initiate the cGAS-STING pathway in keratinocytes. We then addressed whether p53 plays a role in the activation of the p-ATM-p21-cGAS pathway. We tested the protein level of p-p53. As expected, p-p53 was significantly upregulated through 5-FU treatment (Fig. 2H), indicating 5-FU-induced DNA damage could activate the cGAS-STING pathway through p53. Recent studies have shown that chemotherapeutic drugs can induce cellular senescence that causes cancer metastasis and relapse as well as

several other adverse reactions.^{40,41} Furthermore, activated cGAS is associated with cellular senescence.⁴² Therefore, we wanted to verify whether 5-FU induced cellular senescence in keratinocytes. As HaCaT cells do not express the cellular senescence marker beta-galactosidase (SA- β -gal),³² we examined the expression of SA- β -gal in NHEKs and found that SA- β -gal was positively indicated after exposure to 5-FU (Fig. 2I; Fig. S2H). This result was confirmed by staining in the HFS rat model (Fig. S2C). Cellular senescence induced by 5-FU significantly promoted the development of SASP, which in turn activated a severe inflammatory response (Fig. 2G, H). To validate whether the activated cGAS-STING pathway is related to the cellular senescence in keratinocytes. We combined a selective CGAS-STING inhibitor, SN-011 with 5-FU to test the impact of SN-011 in 5-FU-induced cellular senescence. The inhibition of cGAS-STING rescued the senescence phenotype, as evidenced by a decrease in the percentage of SA- β -gal-positive cells (Fig. S4D, G), indicating that the activation of cGAS-STING pathway did cause cellular senescence in keratinocytes. The results showed that DNA damage, which caused the original changes, led to a series of effects including cell cycle arrest, cellular senescence, and inflammation, ultimately resulting in HFS.

TDA provided better protection against the cytotoxicity of 5-FU than TdR in keratinocytes

Based on the above results, we speculated that compensating for dTMP deficiency and facilitating DNA damage repair could be a potential treatment for HFS. By modifying TdR, we synthesized its simplest prodrug, thymidine diacetate (TDA), and tested the efficacies of both TdR and TDA. We used TDA and TdR separately with 5-FU to treat HaCaT cells for 48 h and studied the resulting impacts on 5-FU-induced DNA damage and downstream pathway changes. As shown in Figure 3A–D, TDA produced better protective effects than TdR according to the comet assay and γ H2AX immunofluorescence staining, indicating that TDA could effectively alleviate DNA damage induced by 5-FU. Cell division is arrested in response to DNA damage. Cell cycle analysis was thus performed to evaluate the effects of TdR and TDA. The results in Figure 3E show that TDA significantly relieved the degree of cell cycle arrest, while TdR had little effect. We examined the respective impacts of TDA and TdR on SA- β -gal activity in NHEKs. The results showed that the combination of 5-FU with TDA decreased the number of SA- β -gal-positive cells (Fig. 3F; Fig. S4F). Furthermore, the increased mRNA levels involved in SASP caused by 5-FU, such as those of cyclin E1, p16, p21, p-p53, cGAS, p-IRF3, p-TBK1, IL-1 β , and IL-6, were almost completely reversed by TDA (Fig. 3H), as confirmed by Western blot assay (Fig. 3G; Fig. S4E) and ELISA (Fig. 3I), indicating that TDA has a better effect on 5-FU-induced cytotoxicity and is a potential drug for the treatment of fluoropyrimidine-induced HFS.

at the indicated time points. The heat map illustrates differential gene expression tendency analyses by RT-PCR. The row represents genes and the column represents replicates of each time point. (I) The senescence-associated β -galactosidase activity was assayed in NHEKs after 5-FU (10 μ M) treatment at the indicated time points. Scale bar: 100 μ m. The results in (A), (C) and (E) are presented as the mean \pm SD. * p < 0.05, ** p < 0.01, *** p < 0.001. ns, no significant difference.

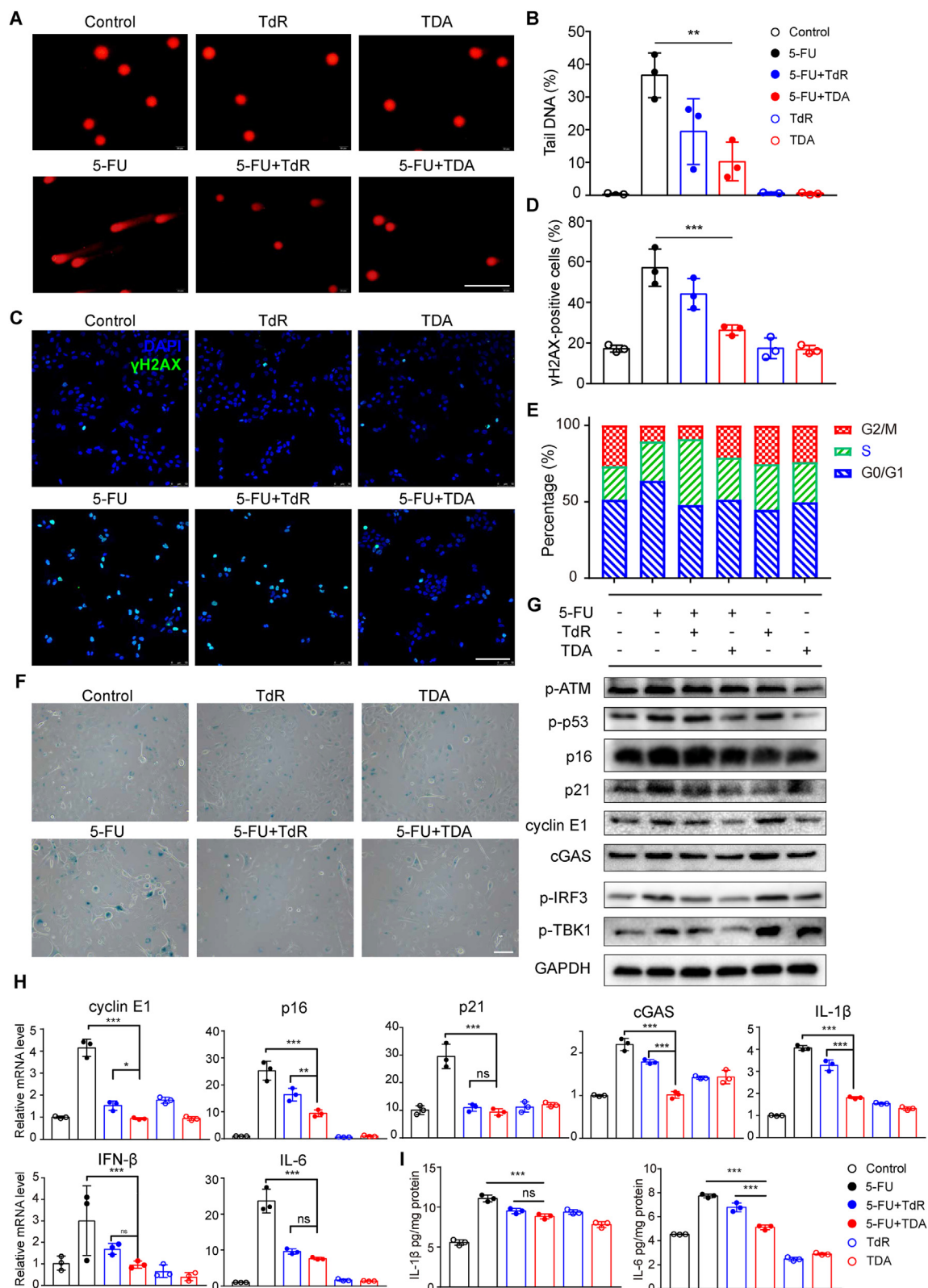


Figure 3 TDA provides better protection against 5-FU-induced cytotoxicity in keratinocytes than TdR. **(A)** Representative images of comet assays and **(B)** the results of comet length analyses ($n = 3$) under different conditions. **(C)** Representative images of γ H2AX immunofluorescence staining and **(D)** the results of γ H2AX positive cell analysis ($n = 3$). **(E)** Populations of cells in G0/G1, S, and G2/M phases under different treatments. **(F)** The senescence-associated β -galactosidase activity was assessed to evaluate the efficacies of TdR and TDA in human primary keratinocytes. **(G)** The expression levels of p-ATM, p-p53, p16, p21, cyclin E1, cGAS, p-IRF3 and p-TBK1 were detected by Western blot assays. **(H)** The transcription levels of p16, p21, cyclin E1, cGAS, p-IRF3, p-TBK1, IL-1 β , IFN- β , and IL-6 were detected by qPCR assays. **(I)** The protein levels of IL-1 β and IL-6 were detected by ELISA assays. Data are presented as mean \pm SD. Statistical significance is indicated by asterisks (*, **, ***, ns) and brackets.

Topical TDA gel successfully relieved HFS induced by capecitabine *in vivo*

Given the observations that compensating for thymidylate deficiency can relieve the DNA damage, cell cycle arrest, cellular senescence, and inflammation induced by 5-FU *in vitro*, we next executed prevention experiments by topically applying antidotes to our rat models of HFS (Fig. 4A). In the prophylactic treatment, TDA showed an excellent protective effect, while TdR performed poorly due to its low permeability. The HFS grade in the TDA group was significantly lower than those in the vehicle and TdR groups (Fig. 4B, C). The probability of grade 2+ rats in the TDA group indicated delays (days) in the progression of HFS severity. The pain tolerance thresholds of rat paws were higher in the TDA group (Fig. 4D), indicating that TDA relieved capecitabine-induced pain reactions in the HFS model. Furthermore, H&E staining and quantification of the epidermis and cuticle thicknesses showed that the damage to the epidermis was relieved by TDA gel application (Fig. 4E; Fig. S5A). Immunohistochemistry analyses showed that the topical application of TDA suppressed the activation of γ H2AX and decreased the expression of cyclin E, p16, and p21 *in vivo*, which demonstrated that TDA decreased DNA damage and cell cycle arrest (Fig. 4F; Fig. S5C). Moreover, TDA significantly decreased the infiltration of lymphocytes and macrophages and the secretion of inflammatory factors (Fig. 4F, I; Fig. S5B–D), which showed that TDA relieved inflammatory responses in capecitabine-induced HFS. Staining for senescence-associated SA- β -gal activity showed that treatment with TDA gel reduced the capecitabine-induced increase in SA- β -gal activity (Fig. 4G; Fig. S5D). In addition, according to Ki67 and EdU staining (Fig. 4F, H), TDA restored the proliferation activity of epidermal basal-layer cells. We also examined the mRNA levels of the cell cycle markers cyclin E1, p16, p21, and cGAS. The increased expression of these genes in the HFS model was reversed by the application of TDA gel (Fig. 4I). Collectively, we concluded that TDA could provide an effective intervention strategy against HFS induced by fluoropyrimidine.

Topical TDA did not alter the antitumor effect of capecitabine *in vivo*

After confirming TDA's ability to alleviate capecitabine-induced HFS, we next tested the impact of the topical application of TDA on the antitumor efficacy of capecitabine using the murine tumor model with the subcutaneous injection of the colorectal carcinoma cell line HCT116. The tumor volumes met the criteria for establishing experimental groups at 24 days after injection. There were no significant differences in tumor volume among the three groups during the initial observation period. We studied the effects of topically applied TDA on the tumor volume, body weight, and tumor weight under oral administration of capecitabine. According to Figure 5A–D, the tumors of

mice treated with capecitabine grew slowly, while the control group displayed rapid tumor growth, but no obvious differences in tumor volume, body weight, or tumor weight between the TDA group and vehicle group were observed. These results indicated that TDA did not influence the antitumor efficacy of capecitabine in nude mice.

Discussion

In the present study, we constructed a rat model of HFS to determine its mechanism. Our findings identified the important role of DNA damage-mediated cellular senescence in keratinocytes in HFS. Mechanistically, DNA damage activates the cGAS-STING pathway, induces cell cycle arrest, and leads to cellular senescence, which promotes the development of SASP and inflammation, ultimately accelerating the onset of HFS. Notably, TDA, which is a prodrug of TdR, was found to be highly effective against fluoropyrimidine-induced HFS (Fig. 6).

The development of a good animal model is critical for exploring the pathogenesis of HFS and assessing the efficacies and risks of novel therapies. By administering several different doses of capecitabine to female and male rats, we successfully constructed an original HFS model in rats, which shared similar skin phenotypes and histological changes with clinical patients in many aspects. Notably, in our HFS rat model and other clinical observations,^{15,17} keratinocytes were the primary cellular target because of the high proliferation rate of keratinocytes. The toxic effect on keratinocytes led to a thinner and frailer epidermis, local inflammatory reactions, and the infiltration of inflammatory cells, ultimately inducing the occurrence of HFS.

Our study confirms that DNA damage-mediated cellular senescence is the main cause of fluoropyrimidine-induced HFS. In comparing TdR and UR, we found that alleviating DNA damage was more effective against 5-FU treatment in HaCaT, indicating that DNA damage is the predominant mechanism of 5-FU toxic action. In comet assays, we observed DNA strand breaks. DNA-directed toxicity causes immediate activation of p53, growth inhibition, cell cycle arrest in the S-phase and cellular senescence, resulting in the induction of SASP. In addition, we observed the same behavior in both the cells and the HFS rat model. Oral gavage of capecitabine significantly induced DNA damage and potentially promoted cellular senescence, and the accumulation of senescent cells contributed to local inflammation. These findings suggest that DNA damage-mediated cellular senescence serves as an activation switch for the inflammatory process and plays a vital role in capecitabine-induced HFS.

Recent studies revealed that self-DNA leaked from the nucleus, which was probably followed by cell division, could activate the cGAS-STING pathway, leading to pathological outcomes.³⁷ Topoisomerase II inhibitors can induce DNA damage and inhibit DNA repair simultaneously, and damaged DNA then activates the cGAS-STING axis to potentiate tumor immunoreaction.³⁸ Likewise, our results

1 β , IL-6 and IFN- β were detected by quantitative RT-PCR ($n = 3$). (I) IL-1 β and IL-6 concentrations in cell culture supernatants were measured by ELISA ($n = 3$). Scale bar: 100 μ m. The results in (B), (D), (H) and (I) are presented as the mean \pm SD. * $P < 0.05$, ** $P < 0.01$, *** $P < 0.001$. ns, no significant difference.

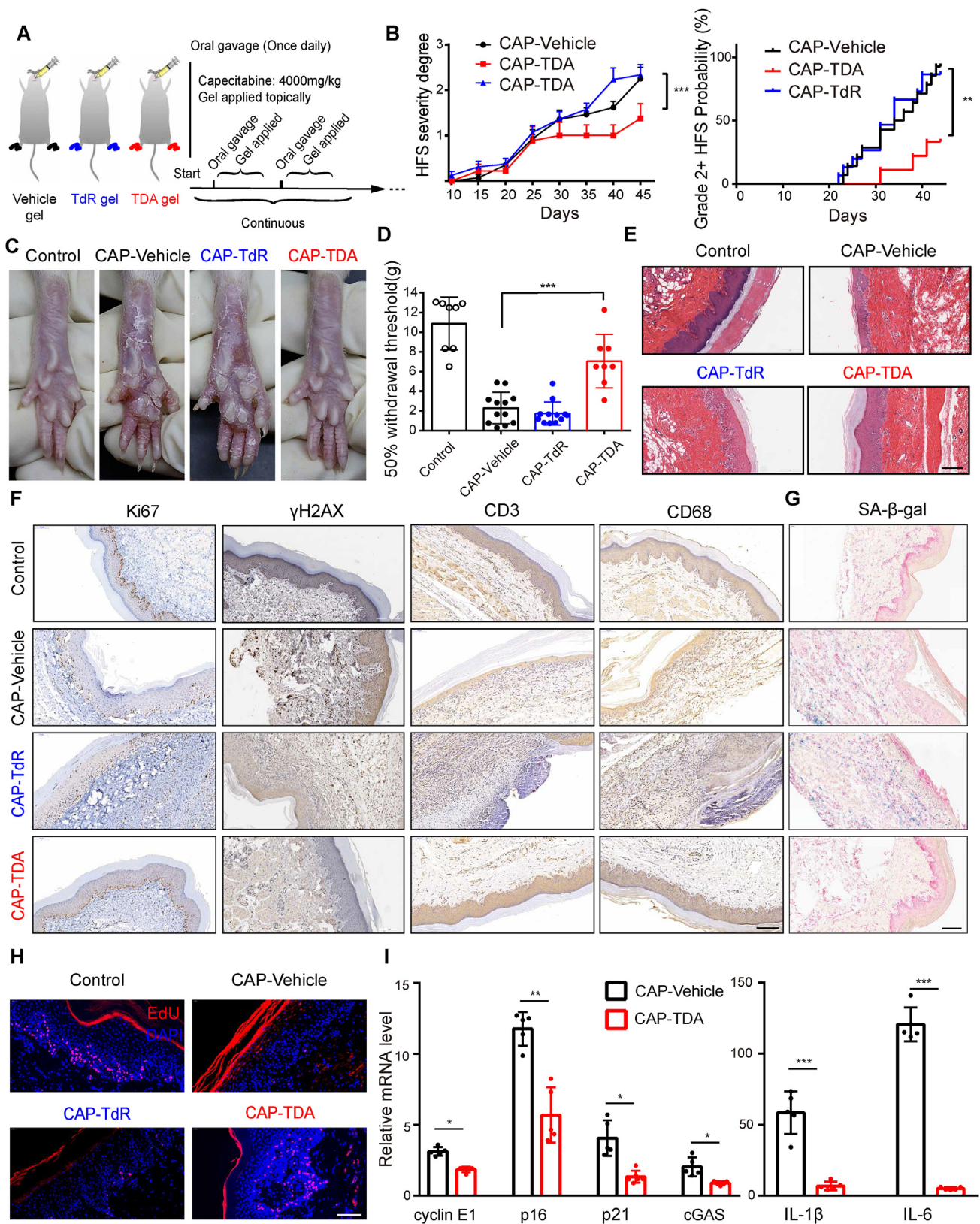


Figure 4 TDA gel relieves capecitabine-induced HFS in a rat model. **(A)** Schematic of the rat experiment methodology. **(B)** Mean HFS grade and grade 2+ HFS probability of rats with the application of TdR or TDA gel. **(C)** Representative images of rat paws. **(D)** Mechanical hypersensitivity in different groups was assayed with von Frey filaments ($n = 8$). **(E)** Representative H&E staining images and **(F)** representative immunohistochemical staining images of Ki67, γ H2AX, CD3 and CD68, of rat paws. **(G)** Intense expression of β -galactosidase was observed in the rat paws. **(H)** EdU immunofluorescence staining of paws. EdU: red; DAPI: blue. **(I)** Transcription

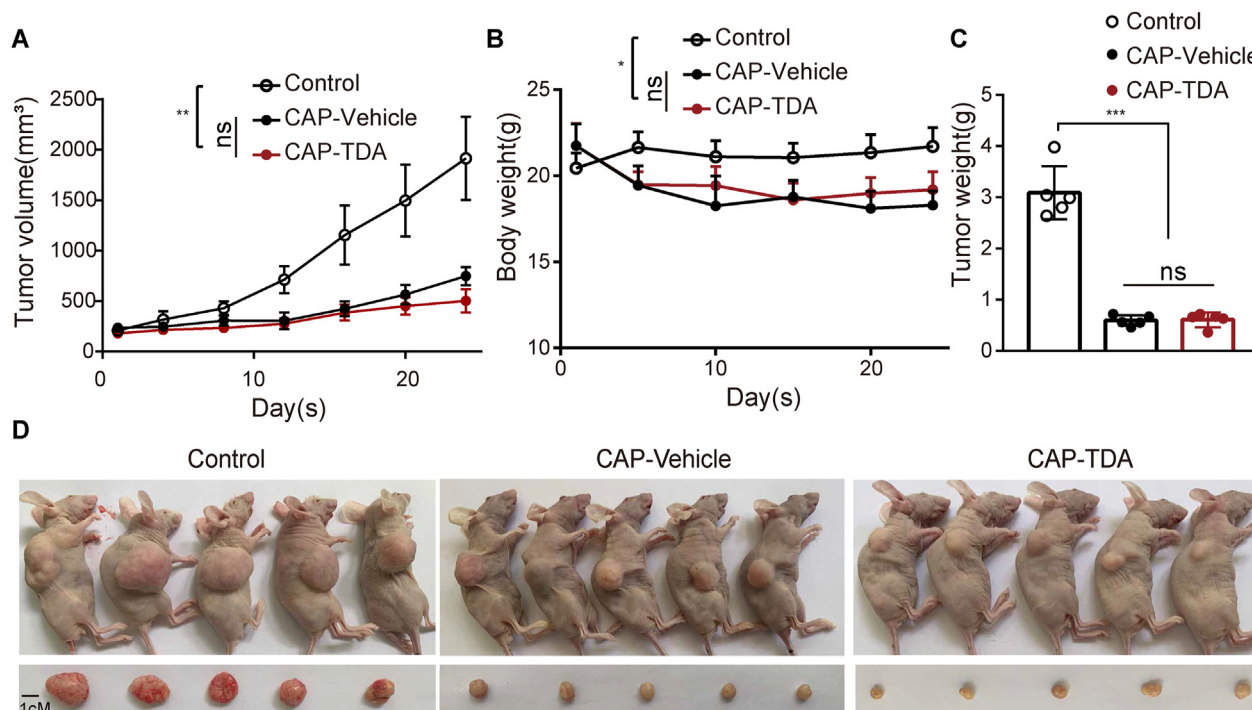


Figure 5 TDA does not affect the antitumor effect of capecitabine. Control: mice were gavaged with solvent. CAP-Vehicle: mice were gavaged with capecitabine 180 mg per kg of body weight and topically treated with vehicle ointment. CAP-TDA: mice were gavaged with capecitabine 180 mg per kg of body weight and topically treated with 5% TDA gel. (A, B) Tumor volume and body weight changes in the HCT116 human colon cancer xenograft models ($n = 5$). (C) Quantitative analysis of tumor weights at the time of sacrifice ($n = 5$). (D) Representative pictures of xenograft tumors from nude mice. The results in (A), (B) and (C) are presented as the mean \pm SD. * $P < 0.05$, ** $P < 0.01$, *** $P < 0.001$. ns, no significant difference.

demonstrated that the cellular signaling pathway of 5-FU-induced DNA damage could be the cGAS-STING pathway. cGAS activation triggers multiple signaling cascades leading to the activation of IRF3 and TBK1. cGAS activation by self-DNA leads to cellular senescence,⁴² mediates the development of SASP, and results in tissue inflammation and toxicity in HFS. Blocking the cGAS-STING pathway could effectively decrease the percentage of senescent cells, indicating the activation of cGAS-STING did cause cellular senescence in keratinocytes. The discovery of this mechanism will advance the understanding of chemotherapy-induced adverse reactions.

The predominant DNA-mediated cytotoxicity of 5-FU implies that reducing DNA damage is a potential intervention strategy in fluoropyrimidine-induced HFS. Our study confirmed that exogenous TdR could compensate for dTMP deficiency and decrease DNA damage. TDA, as a prodrug of TdR synthesized from acetic acid and TdR, was chosen to test its ability to restore cellular physiological functions impaired by 5-FU. As shown in our study, through decreasing the degree of DNA damage, TDA blocked the activation of the p53, cGAS-STING and downstream pathways, and relieved cell cycle arrest, cellular senescence, and inflammation under 5-FU treatment. Owing to the

effectiveness of TDA against 5-FU-induced cytotoxicity in keratinocytes, we determined its efficacy *in vivo* by locally administering TDA. Our study confirmed that topical TDA application could attenuate HFS in rats. Based on the observed favorable outcomes, we believe that topical thymidine prodrugs can be a promising therapeutic strategy for treating fluoropyrimidine-induced HFS.

Topical intervention with TDA effectively mitigated HFS in rat models, and its effects on the anticancer activity of fluoropyrimidine are worth discussion. TdR has been previously proposed as a promising drug to improve the clinical outcomes of patients under 5-FU therapy. Ohnuma et al reported that TdR improved the antitumor efficacy of 5-FU.⁴³ In other systems, the administration of exogenous TdR eliminated 5-FU cytotoxicity.^{44,45} Thus, we tested the influence of TDA on cancer therapy in mice. The results showed that the topical application of TDA exhibited no obvious antagonism of the capecitabine anticancer effect, as evidenced by the tumor volumes, tumor weights, and body weights of mice.

In conclusion, our research revealed a new model of fluoropyrimidine-induced HFS wherein DNA damage-mediated cellular senescence in keratinocytes is largely responsible. We further determined the cGAS-STING

levels of cyclin E1, p16, p21, cGAS, IL-1 β and IL-6 were detected by quantitative RT-PCR ($n = 5$). Scale bar: 100 μ m. The results in (B), (D) and (I) are presented as the mean \pm SD. * $P < 0.05$, ** $P < 0.01$, *** $P < 0.001$. ns, no significant difference.

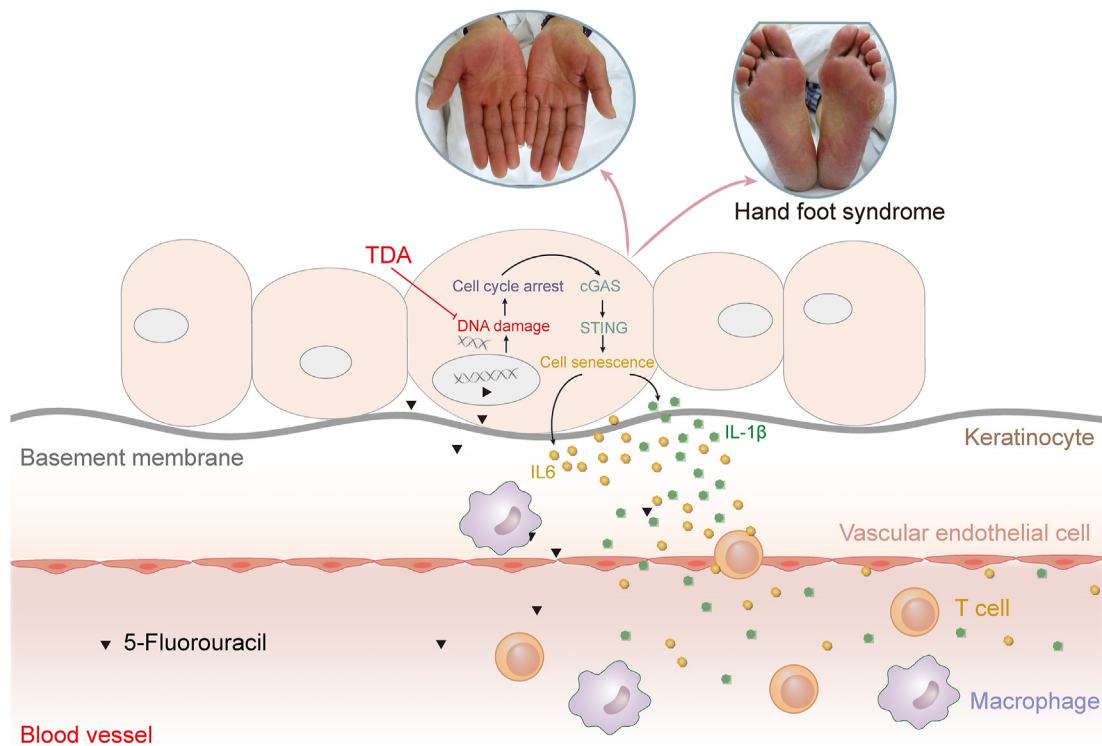


Figure 6 Schematic representation of the mechanism underlying fluoropyrimidine-induced HFS. 5-FU circulates through the bloodstream and enters epidermal cells. DNA damage occurs in keratinocytes upon 5-FU stimulation, subsequently causing cell cycle arrest and activation of the cGAS-STING pathway. Activated cGAS-STING initiates cellular senescence and promotes the secretion of a large number of inflammatory factors, which eventually cause HFS. Supplementation with thymidylate via TDA could reduce DNA damage, thereby effectively reversing capecitabine-induced HFS.

pathway to be the distinct mechanism underlying this toxicity system. More importantly, based on the mechanistic findings, releasing TdR to relieve DNA damage was identified for use against HFS induced by fluoropyrimidines. The topical application of thymidine prodrugs significantly alleviated HFS, which may bring new hope to clinicians and shed new light on the study of drug toxicities.

Author contributions

B.Y. and X.X. performed the experiments and wrote the manuscript. Y.C., J.L. and Y.L. performed some of the *in vitro* experiments. Z.W. and D.L. aided in some animal experiments. J.H. performed xenograft tumor modeling. B.Y. and X.X. performed data analyses. J.L. and S.Z. supervised all experiments. S. Z reviewed and edited the manuscript. All authors approved the final version of the manuscript.

Conflict of interests

The authors declare a Chinese patent application No. 202011192954.0 filed on October 30, 2020. S.Z. and J.L. are shareholders of OnQuality Pharmaceuticals, which develops therapeutics for the treatment of hand-foot syndrome.

Funding

This work was supported by the Youth Thousand Talents Program of China, start-up grants from the Shanghai Jiao Tong University (No. WF220408211). This work was also supported by grants from the State Key Laboratory of Oncogenes and Related Genes (No. 90-17-02) at Shanghai Jiao Tong University and from the Interdisciplinary Program of Shanghai Jiao Tong University (China) (No. YG2017MS18).

Data availability

All data associated with this study are present in the paper or the supplementary materials.

Acknowledgements

We acknowledge Qing You, Yi Lin, and Meng Tian for helpful scientific discussion and manuscript editing. We are thankful to the Shanghai Cancer Institute for the technical platform.

Appendix A. Supplementary data

Supplementary data to this article can be found online at <https://doi.org/10.1016/j.gendis.2022.10.004>.

References

- Heidelberger C, Chaudhuri NK, Danneberg P, et al. Fluorinated pyrimidines, A new class of tumour-inhibitory compounds. *Nature*. 1957;179(4561):663–666.
- Van Cutsem E, Twelves C, Cassidy J, et al. Oral capecitabine compared with intravenous fluorouracil plus leucovorin in patients with metastatic colorectal cancer: results of a large phase III study. *J Clin Oncol*. 2001;19(21):4097–4106.
- Chau I, Norman AR, Cunningham D, et al. A randomised comparison between 6 months of bolus fluorouracil/leucovorin and 12 weeks of protracted venous infusion fluorouracil as adjuvant treatment in colorectal cancer. *Ann Oncol*. 2005;16(4):549–557.
- Son HS, Lee WY, Lee WS, et al. Compliance and effective management of the hand-foot syndrome in colon cancer patients receiving capecitabine as adjuvant chemotherapy. *Yonsei Med J*. 2009;50(6):796–802.
- Heo YS, Chang HM, Kim TW, et al. Hand-foot syndrome in patients treated with capecitabine-containing combination chemotherapy. *J Clin Pharmacol*. 2004;44(10):1166–1172.
- Degen A, Alter M, Schenck F, et al. The hand-foot-syndrome associated with medical tumor therapy - classification and management. *J Dtsch Dermatol Ges*. 2010;8(9):652–661.
- National Cancer Institute, Cancer Therapy Evaluation Program. *Common terminology criteria for adverse events (CTCAE) version 4.03*. 2010.
- Cassidy J, Twelves C, van Cutsem E, et al. First-line oral capecitabine therapy in metastatic colorectal cancer: a favorable safety profile compared with intravenous 5-fluorouracil/leucovorin. *Ann Oncol*. 2002;13(4):566–575.
- Kwakman JJM, Simkens LHJ, van Rooijen JM, et al. Randomized phase III trial of S-1 versus capecitabine in the first-line treatment of metastatic colorectal cancer: SALTO study by the Dutch Colorectal Cancer Group. *Ann Oncol*. 2017;28(6):1288–1293.
- Hong YS, Park YS, Lim HY, et al. S-1 plus oxaliplatin versus capecitabine plus oxaliplatin for first-line treatment of patients with metastatic colorectal cancer: a randomised, non-inferiority phase 3 trial. *Lancet Oncol*. 2012;13(11):1125–1132.
- Milligan ED, Mehmert KK, Hinde JL, et al. Thermal hyperalgesia and mechanical allodynia produced by intrathecal administration of the human immunodeficiency virus-1 (HIV-1) envelope glycoprotein, gp120. *Brain Res*. 2000;861(1):105–116.
- Suzuki S, Nawata S, Inada Y, et al. A cross-sectional survey of methods for controlling hand-foot syndrome in patients receiving capecitabine treatment. *Mol Clin Oncol*. 2018;9(4):443–448.
- Lassere Y, Hoff P. Management of hand-foot syndrome in patients treated with capecitabine (Xeloda). *Eur J Oncol Nurs*. 2004;8(Suppl 1):S31–S40.
- Gressett SM, Stanford BL, Hardwicke F. Management of hand-foot syndrome induced by capecitabine. *J Oncol Pharm Pract*. 2006;12(3):131–141.
- Narasimhan P, Narasimhan S, Hitti IF, et al. Serious hand-and-foot syndrome in black patients treated with capecitabine: report of 3 cases and review of the literature. *Cutis*. 2004;73(2):101–106.
- Chen M, Chen J, Peng X, et al. The contribution of keratinocytes in capecitabine-stimulated hand-foot-syndrome. *Environ Toxicol Pharmacol*. 2017;49:81–88.
- Latif S, Fraga G, Gadzia J. Increased mast cell density in capecitabine-induced hand-foot syndrome: a new pathologic finding. *J Drugs Dermatol JDD*. 2010;9(3):268–270.
- Miller KK, Gorcey L, McLellan BN. Chemotherapy-induced hand-foot syndrome and nail changes: a review of clinical presentation, etiology, pathogenesis, and management. *J Am Acad Dermatol*. 2014;71(4):787–794.
- Kufe DW, Major PP. 5-Fluorouracil incorporation into human breast carcinoma RNA correlates with cytotoxicity. *J Biol Chem*. 1981;256(19):9802–9805.
- Pettersen HS, Visnes T, Vågbo CB, et al. UNG-initiated base excision repair is the major repair route for 5-fluorouracil in DNA, but 5-fluorouracil cytotoxicity depends mainly on RNA incorporation. *Nucleic Acids Res*. 2011;39(19):8430–8444.
- Sobrero AF, Aschele C, Bertino JR. Fluorouracil in colorectal cancer: a tale of two drugs: implications for biochemical modulation. *J Clin Oncol*. 1997;15(1):368–381.
- Aschele C, Sobrero A, Faderan MA, et al. Novel mechanism(s) of resistance to 5-fluorouracil in human colon cancer (HCT-8) sublines following exposure to two different clinically relevant dose schedules. *Cancer Res*. 1992;52(7):1855–1864.
- Guglielmi A, Aschele C, Grossi F, et al. Alternating bolus and continuous infusion 5-fluorouracil: a strategy to overcome resistance to this fluoropyrimidine in advanced colorectal cancer patients. *Cytotechnology*. 1996;19(3):215–219.
- Sobrero AF, Aschele C, Guglielmi AP, et al. Synergism and lack of cross-resistance between short-term and continuous exposure to fluorouracil in human colon adenocarcinoma cells. *J Natl Cancer Inst*. 1993;85(23):1937–1944.
- Glazer RI, Lloyd LS. Association of cell lethality with incorporation of 5-fluorouracil and 5-fluorouridine into nuclear RNA in human colon carcinoma cells in culture. *Mol Pharmacol*. 1982;21(2):468–473.
- Aherne GW, Hardcastle A, Raynaud F, et al. Immunoreactive dUMP and TTP pools as an index of thymidylate synthase inhibition; effect of tomudex (ZD1694) and a non-polyglutamated quinazoline antifolate (CB30900) in L1210 mouse leukaemia cells. *Biochem Pharmacol*. 1996;51(10):1293–1301.
- Hoff PM, Cassidy J, Schmoll HJ. The evolution of fluoropyrimidine therapy: from intravenous to oral. *Oncol*. 2001;6(S4):3–11.
- Chintala L, Vaka S, Baranda J, et al. Capecitabine versus 5-fluorouracil in colorectal cancer: where are we now? *Onco Rev*. 2011;5(2):129–140.
- Cancer MAGI, Lévy E, Piedbois P, et al. Toxicity of fluorouracil in patients with advanced colorectal cancer: effect of administration schedule and prognostic factors. *J Clin Oncol*. 1998;16(11):3537–3541.
- López-Otín C, Blasco MA, Partridge L, et al. The hallmarks of aging. *Cell*. 2013;153(6):1194–1217.
- Surova O, Zhivotovsky B. Various modes of cell death induced by DNA damage. *Oncogene*. 2013;32(33):3789–3797.
- Coppé JP, Patil CK, Rodier F, et al. Senescence-associated secretory phenotypes reveal cell-nonautonomous functions of oncogenic RAS and the p53 tumor suppressor. *PLoS Biol*. 2008;6(12):2853–2868.
- Zhu R, Ji X, Wu X, et al. Melatonin antagonizes ovarian aging via YTHDF2-MAPK-NF- κ B pathway. *Genes Dis*. 2022;9(2):494–509.
- de Keizer PLJ. The fountain of youth by targeting senescent cells? *Trends Mol Med*. 2017;23(1):6–17.
- Carli D, Honorat M, Cohen S, et al. Simultaneous quantification of 5-FU, 5-FUrd, 5-FdUrd, 5-FdUMP, dUMP and TMP in cultured cell models by LC-MS/MS. *J Chromatogr, B: Anal Technol Biomed Life Sci*. 2009;877(27):2937–2944.
- Cahours X, Tran TT, Mesplet N, et al. Analysis of intracellular didanosine triphosphate at sub-ppb level using LC-MS/MS. *J Pharm Biomed Anal*. 2001;26(5–6):819–827.
- Li T, Chen ZJ. The cGAS-cGAMP-STING pathway connects DNA damage to inflammation, senescence, and cancer. *J Exp Med*. 2018;215(5):1287–1299.

38. Wang Z, Chen J, Hu J, et al. cGAS/STING axis mediates a topoisomerase II inhibitor-induced tumor immunogenicity. *J Clin Invest*. 2019;129(11):4850–4862.
39. Marill J, Mohamed Anesary N, Paris S. DNA damage enhancement by radiotherapy-activated hafnium oxide nanoparticles improves cGAS-STING pathway activation in human colorectal cancer cells. *Radiother Oncol*. 2019;141:262–266.
40. Demaria M, O’Leary MN, Chang J, et al. Cellular senescence promotes adverse effects of chemotherapy and cancer relapse. *Cancer Discov*. 2017;7(2):165–176.
41. Wang B, Kohli J, Demaria M. Senescent cells in cancer therapy: friends or foes? *Trends Cancer*. 2020;6(10):838–857.
42. Yang H, Wang H, Ren J, et al. cGAS is essential for cellular senescence. *Proc Natl Acad Sci USA*. 2017;114(23):E4612–E4620.
43. Ohnuma T, Roboz J, Waxman S, et al. Clinical pharmacologic effects of thymidine plus 5-FU. *Cancer Treat Rep*. 1980;64(12):1169–1177.
44. Madoc-Jones H, Bruce WR. On the mechanism of the lethal action of 5-fluorouracil on mouse L cells. *Cancer Res*. 1968;28(10):1976–1981.
45. Reeves Jr WJ, Cailleau R. Mechanism of growth inhibition by 5-fluorouracil. Reversal studies with pyrimidine metabolites *in vitro*. *Proc Soc Exp Biol Med*. 1969;131(3):1068–1072.